Thermal profiles during recrystallization of silicon on insulator with scanning incoherent light line sources

Katsuhiko Kubota, Charles E. Hunt, and Jeffrey Frey
Cornell University School of Electrical Engineering, Ithaca, New York 14853

(Received 24 September 1984; accepted for publication 26 March 1985)

The classical heat equation is solved in one and two dimensions to obtain temperature profiles during recrystallization of silicon thin films on insulators with scanning incoherent light sources. The extent of the Si molten region in multilayered structures is predicted using a macroscopic approach. The enthalpy method incorporates the latent heat of fusion into the temperature-enthalpy relation for Si; the Kirchhoff transformation takes the temperature dependence of the thermal conductivities for the materials into account. The calculations yield the Si melt depths and temperatures and are intended to establish proper experimental conditions.

Various heat sources, including strip heaters,[1] lasers,[2] electron beams,[3] and lamps,[4] have been used to obtain high quality recrystallized silicon on insulator (SOI) materials. For applications such as three-dimensional devices, thermal profile calculations can be used to provide guidelines for the design of SOI fabrication systems, predict optimum combinations of processing conditions, and give a better understanding of experimental results. We describe a method of calculation that incorporates the effects of multilayered structures, heat sources moving with respect to the wafer, temperature dependence of the thermal conductivities, and melting of the Si, using the model shown in Fig. 1.

The heat equation is rewritten with transformed temperatures and enthalpies and solved using a finite-difference method. The Kirchhoff transformation[5] is used to take the temperature dependence of the thermal conductivities into account. The enthalpy method[6] is used to calculate the boundary of the Si molten region in two dimensions without involving the complicated boundary conditions usually associated with a moving solid-liquid interface. A moving coordinate system[7] is employed to effectively cover a widely illuminated region.

The heat equation relates the change in internal energy with time to heat flow by diffusion. Neglecting volume changes, the internal energy change equals that of the enthalpy,[8] leading to the following one-dimensional equations:

$$\frac{\partial H(\Theta(T))}{\partial t} = \frac{\partial^2 \Theta}{\partial x^2} \quad \text{for Si,} \tag{1}$$

$$\frac{\partial h(\theta(T))}{\partial t} = \frac{\partial^2 \theta}{\partial x^2} \quad \text{for SiO}_2, \tag{2}$$

where

$$\Theta(T) = \int k_{\mathrm{Si}}(T')dT'$$

$$\theta(T) = \int k_{\mathrm{SiO_2}}(T')dT'$$

and H is enthalpy (Si), Θ is transformed temperature (Si), k_{Si} is thermal conductivity (Si), h is enthalpy (SiO_2), θ is transformed temperature (SiO_2), $k_{\mathrm{SiO_2}}$ is thermal conductivity (SiO_2), t is time, and x is depth direction. The boundary conditions are

$$-\frac{\partial \Theta}{\partial x} = (1-R)P \quad \text{at top surface} \tag{3}$$

$$\frac{\partial \Theta}{\partial x} = 0 \quad \text{at bottom surface} \tag{4}$$

$$\left.\begin{aligned} \frac{\partial \Theta}{\partial x} &= \frac{\partial \theta}{\partial x} \\ T(\Theta) &= T(\theta) \end{aligned}\right\} \quad \text{at interfaces,} \tag{5}$$

where P and R are the power density and reflectivity, respectively. For samples preheated above the fracture point, and using incident radiation over the wavelength range of interest, simple calculations show that energy absorption is completely at the surface of the top Si layer. Heat loss by radiation and convection, calculated to be less than 100 W/cm^2 even at the Si melting point, is neglected.

A piecewise linear function is used to approximate the temperature-enthalpy relation for Si as shown in Fig. 1(b).

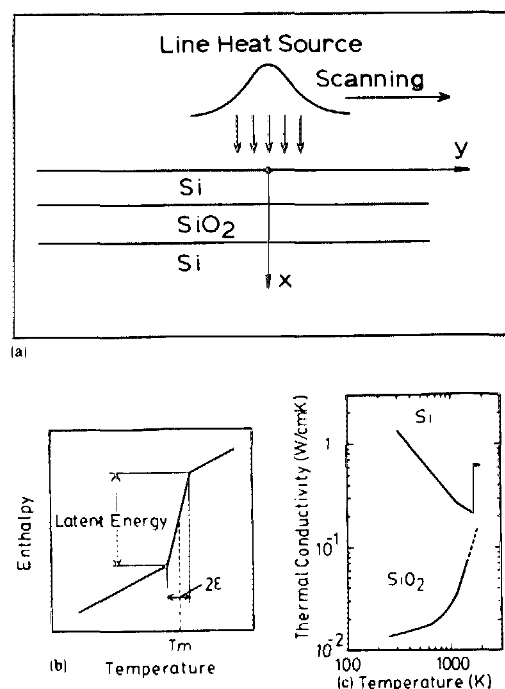

FIG. 1. Schematic illustration for thermal calculation. (a) System model: SOI regrowth with a moving line source; (b) approximated temperature-enthalpy relation for Si. (c) thermal conductivities for Si and SiO_2, used in the calculations.

 0003-6951/85/121153-03$01.00 © 1985 American Institute of Physics

Downloaded 18 Feb 2005 to 169.237.74.43. Redistribution subject to AIP license or copyright, see http://apl.aip.org/apl/copyright.jsp

To facilitate convergence, the melting point is taken as all temperatures within ϵ (= 0.5 K) of 1683 K. The slope within this region is taken as 1660 J/cm^3 K, which is the latent energy of fusion for Si divided by 2ϵ. As the temperature range of interest is expected to be 300–1800 K, the solid and liquid phase heat capacities are both taken as the constant value of 2.21 J/cm^3 K outside of the melting point region of Fig. 1(b). Similarly, a constant enthalpy-temperature slope, with a value of 1.65 J/cm^3 K, is used for SiO_2. This model does not consider microscopic phenomena such as anisotropic growth dependent on crystallographic orientations or constitutional supercooling associated with impurities. The following expressions are used for the thermal conductivity of Si[9]:

$$k_{\mathrm{Si}}(T)=\begin{cases}1521/T^{1.226} & (300\ \mathrm{K}<T<1200\ \mathrm{K})\\ 8.97/T^{0.502} & (1200\ \mathrm{K}<T<1683\ \mathrm{K})\\ 0.64 & (T>1683\ \mathrm{K})\end{cases}\ \frac{\mathrm{W}}{\mathrm{cm\ K}}. \tag{6}$$

As before, the singularity at the melting point is approximated by a steep linear rise within a small temperature range. Based on experimental data,[10] the thermal conductivity of SiO_2 is taken as the following:

$$k_{\mathrm{SiO_2}}(T)=\begin{cases}2.0\times10^{-3}\,T^{0.336} & (300\ \mathrm{K}<T<696\ \mathrm{K})\\ 2.3\times10^{-6}\,T^{1.37} & (696\ \mathrm{K}<T<1149\ \mathrm{K})\\ 7.3\times10^{-11}\,T^{2.84} & (T>1149\ \mathrm{K})\end{cases}\ \frac{\mathrm{W}}{\mathrm{cm\ K}}. \tag{7}$$

Extrapolated values are used above 1400 K.

Temperature-dependent reflectivities were estimated using optical constants available in the literature.[11–13] Above 1200 K, illuminating a 0.5-μm Si/1.0-μm SiO_2/400-μm Si sample with a wavelength of 633 nm, the reflectivity is calculated to be nearly constant at 40% with a rapid increase to 70% at the Si melting point. Adding a 50-nm Si_3N_4 cap reduces the reflectivity, below the melting point, to about 15%, and to 35% above that. A cap is assumed in the calculations since the increased efficiency would be desirable in any real system. The effect of such a thin film on the thermal profiles was taken to be negligible.

One-dimensional calculations were made to verify the algorithms and to provide input parameters for the more precise two-dimensional calculations. Figure 2 shows the results of sample calculations for a temperature rise in a Si/SiO_2/Si sample. The temperatures are seen to increase rapidly and then level off when the top Si layer begins to melt. The absorbed energy is mainly consumed in melting this layer, after which the temperatures rise again until the Si substrate begins to melt. The temperature difference across the SiO_2, which is one of the parameters for process margin, is about 10 K when the top Si layer completely melts. This temperature difference is found to increase with higher power densities, lower initial temperatures, and thicker oxides.

Power density versus time required to melt the top Si layer is plotted in Fig. 3 for various initial wafer temperatures. The curve has an asymptotic slope of -1 for higher power densities and gradually approaches a slope of $-1/2$ as power decreases. Qualitatively, the energy available is the sum of the latent energy for the top Si layer and the energy spread by heat diffusion. The latent heat/power ratio is proportional to time t. If the temperature profile is approximated as a triangle with height equal to the maximum temperature and base equal to the thermal diffusion length, the spread energy has a dependence of $t^{-1/2}$ on the power since the diffusion length varies at $t^{1/2}$. Therefore, with a higher power density, the temperature rise in the vicinity of the sample surface is so fast that the latent energy term dominates.

An appropriate linewidth and scan speed for a given source power density and sample initial temperature may be selected using Fig. 3. A time selected from this figure is approximately the dwell time of the incident power. For the conditions used in Fig. 2 for example, a dwell time of 270 μs is obtained and the scan speed is calculated to be 74 cm/s

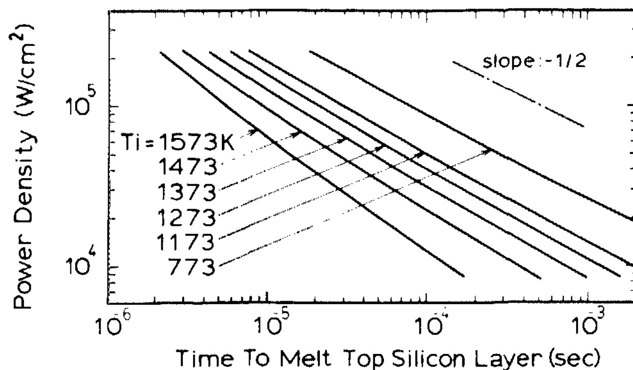

FIG. 2. Temperature rise at three different depths from the sample surface.

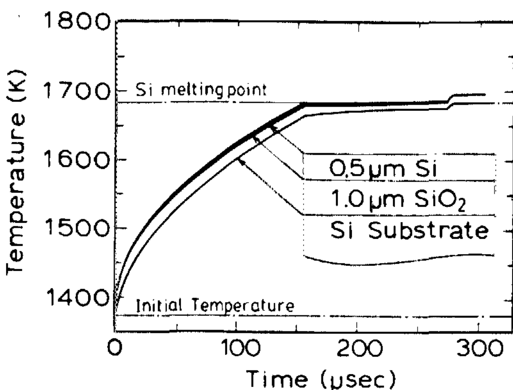

FIG. 3. Power density vs time required to melt top Si layer.

Downloaded 18 Feb 2005 to 169.237.74.43. Redistribution subject to AIP license or copyright, see http://apl.aip.org/apl/copyright.jsp

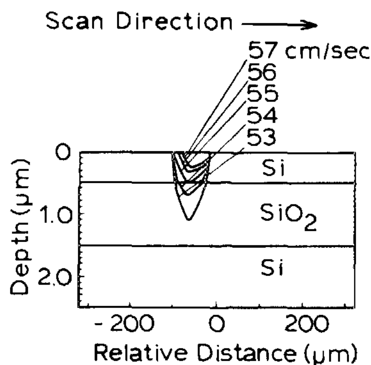

FIG. 4. Isotherms of Si melting point for various scan speeds. $P_{max} = 20$ kW/cm^2, $a = 100\,\mu$m, $T_i = 1373$ K.

with a 0.2-mm-wide heat source. If necessary, these results can be refined using a more accurate two-dimensional calculation.

For the two-dimensional calculation, a coordinate system moving with respect to a sample is used to preferentially allot fine meshes to the region just under the illumination source. Equations (1) and (2) are modified as

$$\frac{\partial H}{\partial t} = \frac{\partial^2 \Theta}{\partial x^2} + \frac{\partial^2 \Theta}{\partial y^2} + v\frac{\partial H}{\partial y}, \tag{1'}$$

$$\frac{\partial h}{\partial t} = \frac{\partial^2 \theta}{\partial x^2} + \frac{\partial^2 \theta}{\partial y^2} + v\frac{\partial h}{\partial y}, \tag{2'}$$

where y is the direction parallel to the translation and v is the scan speed. The incident power density is taken as a Gaussian shape defined as $P = P_{max}\exp(-y^2/a^2)$. In order to cover a wide region of a sample, the boundary condition is

$$T = T_i \text{ at } y = -(vt + 4\sqrt{D_0 t})$$

and

$$y = 4\sqrt{D_0 t}\,, \tag{8}$$

where T_i and D_0 are the initial temperature and heat diffusivity, respectively.

As an example of calculation results, isotherms of the Si melting point are plotted in Fig. 4 for various scan speeds. The elapsed time is 1250 μs, sufficient to establish a steady state. As the scan speed increases, the Si molten region, which lags behind the central point of the heat source, shrinks. The Si molten region just reaches the SiO_2 at a scan speed of 55 cm/s. The value estimated from one-dimensional calculations was 74 cm/s. The difference arises because the maximum temperature along the scan direction occurs inside the envelope $(-a < y < a)$ of the heat source, shortening the effective linewidth. On the basis of additional data, a linewidth correction factor could be developed to allow more accurate calculations using the less expensive one-dimensional model. The shape of the isotherms in the SiO_2 makes the process window small, since the local temperature rapidly rises just after the Si molten region reaches the SiO_2 as shown in Fig. 2.

In conclusion, a thermal calculation method suitable for SOI recrystallization has been presented. The method can be used to predict two-dimensional time-dependent Si molten regions, and is applicable to various kinds of heat sources. With knowledge of accurate temperature profiles during processing, optimum recrystallization conditions can be realized.

The authors would like to thank R. Byrnes for his useful suggestions on computation. This work was supported by the Semiconductor Research Corporation Center of Excellence for Microscience and Technology.

[1]John C. C. Fan, M. W. Geis, and Bor-Yeu Tsaur, Appl. Phys. Lett. **38**, 365 (1981).
[2]K. F. Lee, J. F. Gibbons, K. C. Saraswat, and T. I. Kamins, Appl. Phys. Lett. **35**, 173 (1979).
[3]T. I. Kamins and B. P. Von Herzen, IEEE Electron Device Lett. **EDL-2**, 313 (1981).
[4]T. J. Stultz and J. F. Gibbons, Appl. Phys. Lett. **41**, 824 (1982).
[5]M. Lax, Appl. Phys. Lett. **33**, 786 (1978).
[6]G. H. Meyer, SIAM J. Num. Anal. **10**, 522 (1973).
[7]H. E. Cline, J. Appl. Phys. **54**, 2683 (1983).
[8]N. Shamsundar and E. M. Sparrow, ASME J. Heat Transfer **97**, 333 (1975).
[9]A. E. Bell, RCA Rev. **40**, 295 (1979).
[10]Y. S. Touloukian and E. H. Buyco, *Thermophysical Properties of Matter* (IFI/PLENUM, New York, 1970), Vol. 2.
[11]K. M. Shvarev, B. A. Baum, and P. V. Gel'd, Sov. Phys. Solid State **16**, 2111 (1975).
[12]Y. J. van der Meulen and N. C. Hien, J. Opt. Soc. Am. **64**, 804 (1974).
[13]G. E. Jellison, Jr. and F. A. Modine, Appl. Phys. Lett. **41**, 180 (1982).

Downloaded 18 Feb 2005 to 169.237.74.43. Redistribution subject to AIP license or copyright, see http://apl.aip.org/apl/copyright.jsp